Journal of Statistical Physics, Vol. 88, Nos. 3/4, 1997

Analytic Solutions of Linearized Lattice Boltzmann Equation for Simple Flows

Li-Shi Luo[1]

Received February 27, 1995; final October 30, 1996

A general procedure to obtain analytic solutions of the linearized lattice Boltzmann equation for simple flows is developed. As examples, the solutions for the Poiseuille and the plane Couette flows in two-dimensional space are obtained and studied in detail. The solutions not only have a component which is the solution of the Navier–Stokes equation, they also include a kinetic component which cannot be obtained by the Navier–Stokes equation. The kinetic component of the solutions is due to the finite-mean-free-path effect. Comparison between the analytic results and the numerical results of lattice-gas simulations is made, and they are found to be in accurate agreement.

KEY WORDS: Lattice Boltzmann equation; lattice-gas automata; linearized lattice Boltzmann equation; analytic solutions for the plane Couette and the Poiseuille flows; slip at wall.

I. INTRODUCTION

Recently, there has been a considerable effort in studying the linearized lattice Boltzmann equation (LLBE)[1-5] in the context of lattice gas automata (LGA)[6-9] and the lattice Boltzmann equation (LBE).[10,9] The emphases of previous studies on LLBE have been on the generalized hydrodynamics of LGA and LBE, or the dispersion relations of transport coefficients depending of the wave-vector $\boldsymbol{k}$. It has been shown that LLBE can be used as an effective tool to analyze the validity, as well as the artifacts, of the LGA and LBE hydrodynamics in a quantitative fashion.[1,2]

[1] Complex Systems Group (T-13), MS-B213, Theoretical (T) Division, Los Alamos National Laboratory, Los Alamos, New Mexico 87545; and ICASE, MS 403, NASA Langley Research Center, 6 North Dryden St., Bldg. 1298, Hampton, Virginia 23681-0001; e-mail address: luo@icase.edu.

0022-4715/97/0800-0913$12.50/0

Another useful application of LLBE is to obtain the analytic solutions for simple flows.[1,2] The solutions of LLBE not only contain a component that is the solution of Navier–Stokes equation, but also include a component that is a manifestation of kinetic effect. In this paper, a general procedure to obtain analytic solutions of LLBE is developed. Section II briefly introduces LBE and its hydrodynamics. Section III discusses LLBE. Section IV provides two solutions of LLBE for the Poiseuille flow and the plane Couette flow. Section V presents the numerical results of LGA simulations for the Poiseuille flow and the plane Couette flow. The comparison between the analytic results and the numerical results of lattice-gas simulations is made. Section VI discusses the results and related issues. Finally, an Appendix is included to provide relevant results of the Discrete Fourier Transform used in the Section IV.

II. LATTICE BOLTZMANN EQUATION AND ITS HYDRODYNAMICS

The first LBE model[10] is a straightforward floating-point-number counterpart of the Frisch, Hasslacher, and Pomeau (FHP) LGA model[6,8]:

$$f_\alpha(\boldsymbol{x}+\hat{\boldsymbol{e}}_\alpha, t+1) = f_\alpha(\boldsymbol{x}, t) + \Omega_\alpha \tag{1}$$

where $\hat{\boldsymbol{e}}_\alpha = \cos[(\alpha-1)\pi/3]\,\hat{\boldsymbol{x}} + \sin[(\alpha-1)\pi/3]\,\hat{\boldsymbol{y}}$, $\alpha \in \{1, 2, \ldots, b\}$, are the velocity vectors along the links of the triangular lattice, b is the number of the velocities $\hat{\boldsymbol{e}}_\alpha$ and is equal to 6 for FHP 6-bit models, and Ω is the collision operator. The collision operator Ω in the LBE, Eq. (1), is obtained by replacing the particle number n_α ($n_\alpha \in \{0, 1\}$) by the single particle distribution function f_α ($f_\alpha \equiv \langle n_\alpha \rangle \in [0, 1]$) in the corresponding LGA model. This approximation is called the Boltzmann molecular chaos (*Stosszahlansatz*) or random phase approximation. The replacement of n_α by f_α is justified because the correlations among the n_α's are normally negligible and unimportant for hydrodynamic models.

It can be shown that,[6-8] with the Chapman–Enskog procedure and certain approximations, one can derive the Navier–Stokes equation from Eq. (1):

$$\frac{\partial \boldsymbol{u}}{\partial t} + g(\rho)\,\boldsymbol{u}\cdot\nabla\boldsymbol{u} = -\frac{1}{\rho}\nabla P + \nu\nabla^2\boldsymbol{u} \tag{2}$$

where ν is the kinetic viscosity depending on the eigenvalues of the collision operator Ω,[1,2] and the factor $g(\rho)$ reflects the lack of Galilean invariance

in LGA models at microscopic level, but Galilean invariance can be restored by rescaling t, ν, and P.[8, 2]

In the situation where a constant body force (or gravity), $\boldsymbol{F}$, is present, the Navier–Stokes equation becomes:

$$\frac{\partial \boldsymbol{u}}{\partial t} + g(\rho)\, \boldsymbol{u} \cdot \nabla \boldsymbol{u} = -\frac{1}{\rho} \nabla P + \nu \nabla^2 \boldsymbol{u} + \frac{1}{\rho} \boldsymbol{F} \tag{3}$$

The corresponding forcing scheme in the LBE method,

$$f_\alpha(\boldsymbol{x} + \hat{\boldsymbol{e}}_\alpha, t+1) = f_\alpha(\boldsymbol{x}, t) + \Omega_\alpha + F_\alpha \tag{4}$$

must satisfy the following criteria:

$$\sum_\alpha F_\alpha = 0 \tag{5a}$$

$$\sum_\alpha \hat{\boldsymbol{e}}_{\alpha, i} F_\alpha = F_i \tag{5b}$$

$$\sum_\alpha \hat{\boldsymbol{e}}_{\alpha, i} \hat{\boldsymbol{e}}_{\alpha, j} F_\alpha = 0 \tag{5c}$$

where the Latin subscript i or j denotes the Cartesian coordinate x or y. For FHP 6-bit models one choice of F_α satisfying the above criteria is:

$$F_\alpha = \frac{D}{b} \boldsymbol{F} \cdot \hat{\boldsymbol{e}}_\alpha \tag{6}$$

where $b = 6$, and D is the dimension of the space.

III. LINEARIZED LATTICE BOLTZMANN EQUATION

Assuming that $f_\alpha(\boldsymbol{x}, t) = d(1 + \phi_\alpha(\boldsymbol{x}, t))$ with $|\phi_\alpha| \ll 1$, where d is the equilibrium density per direction at zero mean velocity, we can linearize Eq. (1) to obtain

$$\phi_\alpha(\boldsymbol{x} + \hat{\boldsymbol{e}}_\alpha, t+1) = \phi_\alpha(\boldsymbol{x}, t) + \sum_\beta \mathbb{J}_{\alpha\beta} \phi_\beta(\boldsymbol{x}, t) \tag{7}$$

where J is the Jacobian matrix of Ω.

The Fourier transform of Eq. (7) in space is

$$\tilde{\phi}_\alpha(\boldsymbol{k}, t+1) = e^{i\boldsymbol{k} \cdot \hat{\boldsymbol{e}}_\alpha} \sum_\beta (\delta_{\alpha\beta} + \mathbb{J}_{\alpha\beta})\, \tilde{\phi}_\beta(\boldsymbol{k}, t) \tag{8}$$

The above equation can be written in a vector form:

$$|\tilde{\phi}(\boldsymbol{k}, t+1)\rangle = \mathbb{H}(\boldsymbol{k})\, |\tilde{\phi}(\boldsymbol{k}, t)\rangle \tag{9}$$

where $|\tilde{\phi}(\boldsymbol{k}, t)\rangle$ is the fluctuation vector with component $\tilde{\phi}_\alpha(\boldsymbol{k}, t)$, i.e.,

$$|\tilde{\phi}(\boldsymbol{k}, t)\rangle = (\tilde{\phi}_1, \tilde{\phi}_2, \tilde{\phi}_3, \tilde{\phi}_4, \tilde{\phi}_5, \tilde{\phi}_6)^T$$

The matrix

$$\mathbb{H}(\boldsymbol{k}) = \mathbb{D}(\boldsymbol{k})\, \mathbb{H}_0 \tag{10}$$

is the evolution operator, where

$$\mathbb{H}_0 = \mathbb{I} + \mathbb{J} \tag{11}$$

and I is the identity matrix. The diagonal matrix

$$\mathbb{D}(\boldsymbol{k}) = \mathbf{diag}(e^{i\boldsymbol{k}\cdot\hat{\boldsymbol{e}}_1}, e^{i\boldsymbol{k}\cdot\hat{\boldsymbol{e}}_2}, \ldots, e^{i\boldsymbol{k}\cdot\hat{\boldsymbol{e}}_6}) \tag{12}$$

is the displacement operator

The eigenmodes of $\mathbb{H}(\boldsymbol{k})$ are the hydrodynamic and kinetic modes, and the eigenvalues of $\mathbb{H}(\boldsymbol{k})$ are related to the transport coefficients of the corresponding LGA or LBE model.[1,2] By solving the eigenvalue problem of $\mathbb{H}(\boldsymbol{k})$, one can study the generalized hydrodynamics of the model.[1-3]

IV. ANALYTIC SOLUTIONS OF LINEARIZED LATTICE BOLTZMANN EQUATION

Even though the eigenvalue problem of $\mathbb{H}(\boldsymbol{k})$ cannot be solved analytically in general, the inverse of $\mathbb{H}(\boldsymbol{k})$ can always be obtained exactly. Therefore, one can obtain analytic solutions for some flows in which the boundary conditions and forcing are simple. Although the procedure to obtain the solution of LLBE (with appropriate boundary conditions) is general, it will be illustrated using the 6-bit collision-saturated nondeterministic FHP model, including all possible two-, three-, and four-body collisions. In this case, $\mathbb{H}_0$ is a circulant matrix[11] and is given by:

$$\mathbb{H}_0 = \mathbf{circ}[h_1, h_2, h_3, h_4, h_3, h_2] \tag{13}$$

where $h_1 = 1 - \tilde{d}(1 + 3\tilde{d})$, $h_2 = \tilde{d}(1 + 4\tilde{d})/2$, $h_3 = \tilde{d}/2$, $h_4 = -\tilde{d}(1 + \tilde{d})$, and $\tilde{d} = d(1 - d)$.

Assuming that the system is driven by a time-independent force, whose Fourier transform is $|\tilde{F}(\boldsymbol{k})\rangle = (\tilde{F}_1(\boldsymbol{k}), \tilde{F}_2(\boldsymbol{k}),..., \tilde{F}_6(\boldsymbol{k}))^T$, and that a time-independent solution exists:

$$|\tilde{\phi}(\boldsymbol{k}, t+1)\rangle = |\tilde{\phi}(\boldsymbol{k}, t)\rangle = |\tilde{\phi}(\boldsymbol{k})\rangle$$

then Eq. (9) becomes:

$$|\tilde{\phi}(\boldsymbol{k})\rangle = \mathbb{H}(\boldsymbol{k})\,|\tilde{\phi}(\boldsymbol{k})\rangle + \mathbb{D}(\boldsymbol{k})\,|\tilde{F}(\boldsymbol{k})\rangle \tag{14}$$

The solution of the above equation is

$$|\tilde{\phi}(\boldsymbol{k})\rangle = [\mathbb{I} - \mathbb{H}(\boldsymbol{k})^{-1}]\,\mathbb{D}(\boldsymbol{k})\,|\tilde{F}(\boldsymbol{k})\rangle \tag{15}$$

Therefore, by specifying $|\tilde{F}(\boldsymbol{k})\rangle$ (or $|F(\boldsymbol{x})\rangle$ equivalently), one can always obtain $|\tilde{\phi}(\boldsymbol{k})\rangle$ analytically, as well as the flow profile. In what follows, two simple flows are analyzed: the Poiseuille flow and the plane Couette flow in the two-dimensional space.

A. Poiseuille Flow

The Poiseuille flow is the uniformly forced flow between two parallel plates.[12] In the following analysis, the flow (in the two-dimensional space) considered is in the interval $[0, L]$ on the y-axis, with periodic boundary conditions in both $\hat{x}$ and $\hat{y}$ directions. We shall apply Discrete Fourier Transform (DFT) (see the Appendix or ref. 13) of a set of N discrete data points in the interval $[0, L]$, and denote $w_N = \exp(i2\pi/N)$, $\delta_y = L/N$, $k_y = k\pi$, and $y = nL/N$. For the sake of convenience, we also assume $L = 2$.

The forcing function in the Poiseuille flow is a square-wave function along x-axis, i.e., $\boldsymbol{F}(\boldsymbol{x}) = F(y)\,\hat{x}$, where

$$F(y) = \begin{cases} F_0, & 0 \leqslant y < 1 \\ -F_0, & 1 \leqslant y < 2 \end{cases} \tag{16}$$

That is, $|F(y)\rangle = |\hat{e}_{\alpha,x}\rangle\, F(y)$, where

$$|\hat{e}_{\alpha,x}\rangle = (\hat{e}_{1,x}, \hat{e}_{2,x},..., \hat{e}_{6,x})^T = (1,\ 1/2,\ -1/2,\ -1,\ -1/2,\ 1/2)^T$$

For the above forcing function, the DFT of $F(y)$ is:

$$\tilde{F}(2k+1) = \frac{4F_0}{1 - w_N^{2k+1}}, \qquad 0 \leqslant k \leqslant N/2 - 1 \tag{17}$$

Therefore, the DFT of the x-momentum, p_x, is

$$\tilde{p}_x(k) = \langle \hat{\boldsymbol{e}}_{\alpha,x} | \tilde{\boldsymbol{\phi}}(\boldsymbol{k}) \rangle = \langle \hat{\boldsymbol{e}}_{\alpha,x} | [\mathbb{I} - \mathbb{H}(\boldsymbol{k})]^{-1} \mathbb{D}(\boldsymbol{k}) | \hat{\boldsymbol{e}}_{\alpha,x} \rangle \tilde{F}(k_y) \quad (18)$$

where $\boldsymbol{k}$ is orthogonal to the direction of forcing, $\boldsymbol{F}$. Henceforth,

$$\langle \hat{\boldsymbol{e}}_{\alpha,x} | [\mathbb{I} - \mathbb{H}(\boldsymbol{k})]^{-1} \mathbb{D}(\boldsymbol{k}) | \hat{\boldsymbol{e}}_{\alpha,x} \rangle = a + \frac{3b}{2 \sin^2(k_y \delta_y/2)} \quad (19)$$

where

$$a = \frac{2\lambda_3 + 3\lambda_4 - 1}{(1+\lambda_3)(1-\lambda_4)} = \frac{(2 - 3\tilde{d} - 15\tilde{d}^2)}{3\tilde{d}^2(2 - 3\tilde{d} - 6\tilde{d}^2)} \quad (20a)$$

$$b = \frac{1-\lambda_3}{1+\lambda_3} = \frac{3\tilde{d}(1+2\tilde{d})}{(2 - 3\tilde{d} - 6\tilde{d}^2)} = \frac{1}{8\nu} \quad (20b)$$

and

$$\lambda_3 = 1 - 3\tilde{d}(1+2\tilde{d}) \quad (21a)$$

$$\lambda_4 = 1 - 6\tilde{d}^2 \quad (21b)$$

are the eigenvalues of $\mathbb{H}_0$ corresponding to the two kinetic modes of H_0.[1,2] Therefore, from Eqs. (17), (18), and (19), and with $y = (2n+1)/N$, where $n \in \{0, 1, \ldots, N-1\}$, we obtain (see details in the Appendix):

$$p_x(y) = \frac{1}{N} \sum_{k=0}^{N/2-1} \tilde{p}_x(k)\, w_N^{-(2k+1)n} = \begin{cases} p_0 y(1-y) + \Delta p, & 0 < y < 1 \\ p_0 (y-1)(y-2) - \Delta p, & 1 < y < 2 \end{cases} \quad (22)$$

where

$$p_0 = \frac{3}{4} b N^2 F_0 = \frac{L_y^2 F_0}{8\nu} \quad (23a)$$

$$\Delta p = \frac{1}{4} (4a + 3b)\, F_0 \quad (23b)$$

and $L_y = \sqrt{3}\, N/2$ is twice of the channel width between the two plates in lattice gas simulation.

The term Δp in Eq. (22) represents a slip at boundary. In the continuum limit ($N \to \infty, d \to 0$) and with an appropriate scaling between N and d, i.e., $d \to d_0/N^{2/3}$, where d_0 is a constant,

$$a \sim \frac{2}{3d^2} \tag{24a}$$

$$b \sim \frac{3d}{2} \tag{24b}$$

then

$$\lim_{\substack{N \to \infty \\ d \to d_0/N^{2/3}}} \frac{p_x(y)}{N^{4/3}} = \bar{p}_x(y) = \begin{cases} \bar{p}_0 y(1-y) + \Delta\bar{p}, & 0 < y < 1 \\ \bar{p}_0(y-1)(y-2) - \Delta\bar{p}, & 1 < y < 2 \end{cases} \tag{25}$$

where

$$\bar{p}_0 = \frac{9d_0}{4} F_0 \tag{26a}$$

$$\Delta\bar{p} = \frac{2}{3d_0^2} F_0 \tag{26b}$$

Therefore, with an appropriate scaling between N and d, the slip exists under the continuum limit.

A few comments are in order for the slip momentum Δp. It is obvious that in the low density limit $d \to 0$,

$$\Delta p \sim d^{-2} \sim l^2 \tag{27}$$

where l is the mean-free-path.[4, 15] This means that the slip is related to the mean-free-path l (or Knudsen number K_n) in the low density limit. In other words, the slip velocity would diminish as the mean-free-path (or Knudsen number K_n) goes to zero in the limit of $N \to \infty$ while the density d is remained as a constant. The slip phenomenon has been studied since the time of Maxwell,[16] and there exit recent results of molecular dynamics (MD) simulations to study to slip.[17, 18] Our results here qualitatively confirm the previous results of MD simulations in term of the dependence of the slip on the mean-free-path (or Knudsen number K_n).[17]

B. Plane Couette Flow

The plane Couette flow is the flow between two parallel plates moving in opposite directions with constant speeds. In the case considered here, the two plates move in opposite directions, but with the same speed. The forcing term for the plane Couette flow is

$$\boldsymbol{F}(y) = F_0[\delta(y) - \delta(y-1)]\,\hat{\boldsymbol{x}} \tag{28}$$

The DFT of the above forcing function is

$$\tilde{F}(2k+1) = 2F_0,\ 0 \leqslant k \leqslant N/2 - 1 \tag{29}$$

Then, the DFT of the x-momentum is

$$\tilde{p}_x(k) = \langle \hat{\boldsymbol{e}}_{\alpha,x} | [\mathbb{I} - \mathbb{H}(\boldsymbol{k})]^{-1}\, \mathbb{D}(\boldsymbol{k})\, | \hat{\boldsymbol{e}}_{\alpha,x} \rangle\, \tilde{F}(k) = 2F_0 \left(a + \frac{3b}{2\sin^2(k_y \delta_y/2)} \right) \tag{30}$$

and the inverse DFT of the x-momentum across the channel is (see details in the Appendix):

$$p_x(y) = \frac{1}{N} \sum_{k=0}^{N/2-1} \tilde{p}_x(k)\, w_N^{-(2k+1)n} = \begin{cases} (p_0 + \Delta p), & y = 0 \\ p_0(1-2y), & 0 < y < 1 \\ -(p_0 + \Delta p), & y = 1 \\ p_0(2y-3), & 1 < y < 2 \end{cases} \tag{31}$$

where $y = (2n+1)/N$, $n \in \{0, 1, \ldots, N-1\}$,

$$p_0 = \tfrac{3}{4} b N F_0 \tag{32a}$$

$$\Delta p = a F_0 \tag{32b}$$

and a and b are given by Eq. (20). Again, the above equation shows that the momentum profile has a slip (discontinuity) at wall. Similar to the Poiseuille flow, the slip exits under the continuum limit $N \to \infty$ and $d \to d_0/N^{1/3}$, where d_0 is a constant,

$$\lim_{\substack{N \to \infty \\ d \to d_0/N^{1/3}}} \frac{p_x(y)}{N^{2/3}} = \bar{p}_x(y) = \begin{cases} (\bar{p}_0 + \Delta\bar{p}), & y = 0 \\ \bar{p}_0(1-2y), & 0 < y < 1 \\ -(\bar{p}_0 + \Delta\bar{p}), & y = 1 \\ \bar{p}_0(2y-3), & 1 < y < 2 \end{cases} \tag{33}$$

where $\bar{p}_0$ and $\Delta\bar{p}$ are given by Eq. (26), with a different d_0. The distinction between the plane Couette flow and the Poiseuille flow in the continuum limit is that the scaling between N and d is different under the continuum limit. This difference is apparently due to the difference in the forcing: For the Poiseuille flow the forcing is two-dimensional, whereas for the Couette flow it is one-dimensional.

V. NUMERICAL RESULTS

Numerical simulations with 6-bit FHP LGA model are performed to test the accuracy of the linearized theory. The analytic results are compared with results of LGA simulations. The setup of the LGA simulation for the Poiseuille flow is as follows: The plates are placed parallel to the velocity direction ($\hat{\boldsymbol{e}}_1$) and periodic boundary conditions are applied. The system size is $N_x \times N_y = 512 \times 32$. The forcing is a square-wave function between the plates. It is of uniform magnitude on sites $1 \leqslant y \leqslant N_y/2$ and of opposite uniform magnitude on sites $N_y/2 + 1 \leqslant y \leqslant N_y$.

For the LGA simulations, the microscopic rules of applying uniform body force are described in Fig. (1). The uniform body force is achieved by assigning a random number r, $0 \leqslant r \leqslant 1$, to each site at each time step, after collision and advection process have taken place, the microscopic forcing rules described in Fig. 1 are executed if $r \leqslant r_0$ and if the rule is allowed at a particular site. The forcing magnitude, F_0, is related to the probability r_0 by

$$F_0 = 2r_0\, d(1-d) \tag{34}$$

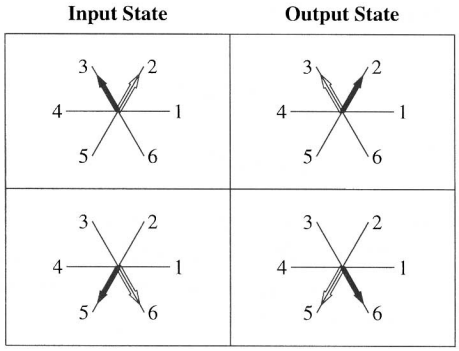

Fig. 1. Forcing rules of FHP 6-bit models. In the left column are the states before the forcing. Those in the right column are after forcing. Each successful application of the forcing rule adds one unit of momentum to the system. The solid arrows indicate occupied states while the hollow ones indicate vacant states. States not indicated may be either occupied or vacant.

for the forcing rules of Fig. 1.[8] Upon each successful forcing application, the system gains one unit of momentum in the $\hat{x}$ direction. The momentum profile is obtained by averaging over x direction and an interval of time after a number of iterations initially.

In Fig. 2, the momentum profile of the forced flow between parallel plates (the Poiseuille flow)[12] from the above analysis and LGA simulations are compared. Note that, in Fig. 2, the discontinuity of the momentum profiles at the boundaries (the slip momentum) is accurately predicted by the analysis. This phenomenon is a manifestation of the kinetic effect due to a finite mean-free-path.[17, 18]

In Fig. 3, the momentum profile of the plane Couette flow from the above analysis and LGA simulations are compared. The arrangement for the LGA simulation of the Couette flow is the same as for the Poiseuille flow, but the uniform forcing is only applied on two rows: $y=1$ and $y=N/2+1$, with the same magnitude and opposite directions. The system size for this simulations is $N_x \times N_y = 16384 \times 32$. The momentum profile is obtained by averaging over x direction and an interval of time after a number of iterations initially. Although the slip along the boundary is well captured by the theoretical analysis, a systematic discrepancy between the analytic result (straight line) and the numerical result from the LGA

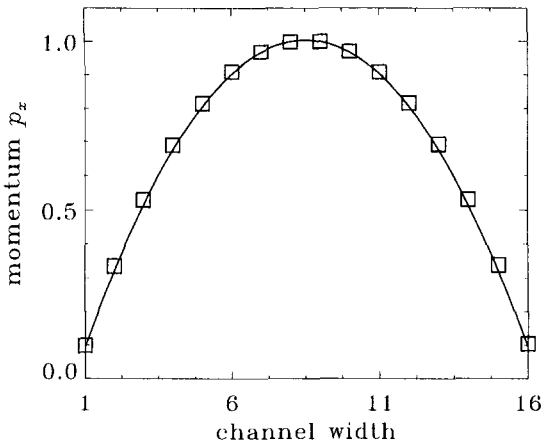

Fig. 2. Momentum profile of Poiseuille flow for density per link $d=0.2$ and a channel width of 16 lattice sites. The system size is $N_x \times N_y = 512 \times 32$. To obtain a steady state, 10^6 time iterations were run before the averaging. The momentum p_x is averaged over N_x and over 2×10^6 time iterations. The analytic result of Eq. (22) is represented by the solid line and the LGA simulation by □. The graph is rescaled so that $p_{max}=1$. Note the agreement for the non-zero momentum at the walls (slip velocity) due to finite mean free path. The simulation was run on a CRAY Y-MP, with the forcing magnitude $F_0 \approx 1.0641 \times 10^{-3}$.

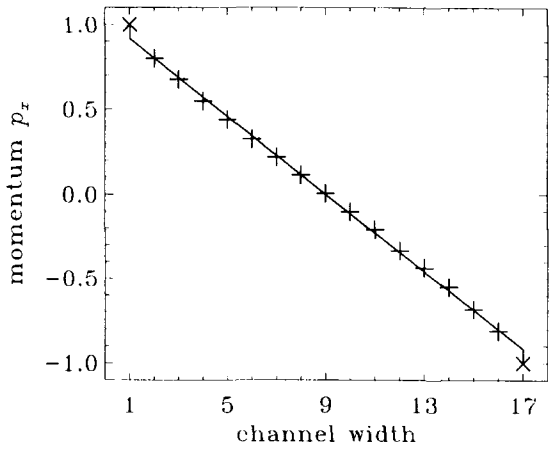

Fig. 3. Momentum profile of plane Couette flow for density per link $d = 0.2$ and a channel width of 16 lattice sites. The system size is $N_x \times N_y = 16384 \times 32$. The probability of applying forcing is 0.06. To obtain a steady state, 10^3 time iterations were run before the averaging. The momentum, p_x, is averaged over N_x and over 2×10^3 time iterations. The analytic result of Eq. (31) is represented by the solid line and the LGA simulation by "$\times$" and "+". The graph is rescaled so that $p_{\max} = 1$. The simulation was run on a CM-200 computer.

simulation (plus signs) is observed. The discrepancy can be attributed to the linearization of the collision operator, which is the only approximation made in our analysis.

VI. CONCLUSION AND DISCUSSION

The analysis and numerical findings presented here confirm what has been found in molecular dynamics simulations in terms of the dependence of the slip momentum on mean-free-path l or Knudsen number K_n.[17, 18] Our theoretical analysis is also consistent with the theoretical results in ref. 19. In more general terms, our results demonstrate that hydrodynamics does apply quantitatively in very small scales comparable to the mean-free-path in the system.[20, 21] However, kinetic effects are also visible in the small scales. Furthermore, it has been shown that, for both the Poiseuille flow and the plane Couette flow modeled by lattice-gas automata, velocity profiles for the both flows consist a part which satisfies the Navier–Stokes equation, and a part (the slip at wall) which is due to the kinetic effect of a finite mean-free-path and cannot be described by the Navier–Stokes equation.[12]

In conclusion, solutions of the linearized lattice Boltzmann equation for simple flows can be obtained analytically with the method described in

this paper. The kinetic effects due to a finite mean-free-path have been analyzed quantitatively, and accurate agreements with LGA simulations were found. The method described here can certainly be applied to other LGA or LBE models in two or three dimensions.

APPENDIX: DISCRETE FOURIER TRANSFORM

The discrete Fourier Transform (DFT) of a set of N data points, $f_n \equiv f(x_n)$, in the interval $x \in [0, L]$, is defined as

$$\tilde{f}_k = \sum_{n=0}^{N-1} f_n w_N^{kn}, \qquad \text{for} \quad 0 \leqslant k \leqslant N-1 \tag{A1}$$

where $\tilde{f}_k \equiv \tilde{f}(k)$, and $w_N \equiv \exp(i2\pi/N)$. The inverse DFT is

$$f_n = \frac{1}{N} \sum_{k=0}^{N-1} \tilde{f}_k w_N^{-kn}, \qquad \text{for} \quad 0 \leqslant n \leqslant N-1 \tag{A2}$$

If N is even and $f_{n+N/2} = -f_n$, then

$$\tilde{f}_{2k} = 0 \tag{A3}$$

$$\tilde{f}_{2k+1} = 2 \sum_{n=0}^{N/2-1} f_n w_N^{(2k+1)n}, \qquad \text{for} \quad 0 \leqslant k \leqslant N/2-1 \tag{A4}$$

With the following results,

$$\sum_{n=0}^{M-1} r^n = \frac{1-r^M}{1-r} \tag{A5a}$$

$$\sum_{n=0}^{M-1} n r^n = \frac{r(1-r^M)}{(1-r)^2} - \frac{Mr^M}{1-r} \tag{A5b}$$

$$\sum_{n=0}^{M-1} n^2 r^2 = \frac{2r(1-r^m)}{(1-r)^3} - \frac{r(1+(2M-1)\,r^M)}{(1-r)^2} - \frac{M^2 r^M}{1-r} \tag{A5c}$$

and with the substitutions of $M = N/2$ and $r = w_N^{2k+1}$, we can obtain the following DFT's for $0 \leqslant k \leqslant N/2-1$:

$$f_n = \delta(n), \qquad \tilde{f}_{2k+1} = 2 \tag{A6a}$$

$$f_n = 1, \qquad \tilde{f}_{2k+1} = \frac{4}{1 - w_N^{2k+1}} \tag{A6b}$$

$$f_n = n, \qquad \tilde{f}_{2k+1} = \frac{N}{1 - w_N^{2k+1}} + \frac{4w_N^{2k+1}}{(1 - w_N^{2k+1})^2} \tag{A6c}$$

$$f_n = n^2, \qquad \tilde{f}_{2k+1} = \frac{N^2}{2(1 - w_N^{2k+1})} + \frac{2(N-2)\, w_N^{2k+1}}{(1 - w_N^{2k+1})^2} + \frac{8w_N^{2k+1}}{(1 - w_N^{2k+1})^3} \tag{A6d}$$

and the following inverse DFT's for $0 \leqslant n \leqslant N/2 - 1$:

$$\tilde{f}_{2k+1} = -\frac{4w_N^{2k+1}}{(1 - w_N^{2k+1})^2} = \frac{1}{\sin^2(\pi(2k+1)/N)}, \qquad f_n = \frac{N - 4n}{4} \tag{A7}$$

$$\tilde{f}_{2k+1} = -\frac{16w_N^{2k+1}}{(1 - w_N^{2k+1})^3}, \qquad f_n = -2n^2 + (N-2)\, n + N/2 \tag{A8}$$

With the above results and the substitution of $y = (2n+1)/N$, the results of momentum profiles in Section IV can be easily obtained.

ACKNOWLEDGMENTS

The author would like express his gratitude to Dr. Gary D. Doolen for his ever-lasting support, guidance, and encouragement. The author especially likes to thank Prof. D. d'Humières for his diligence in reviewing this paper and his helpful comments and suggestions regarding the DFT. The author would also like to thank Dr. Shiyi Chen for his support of this work, Dr. Hudong Chen, Prof. Y. C. Lee, and Dr. H. Rose for many enlightening discussions, and Mr. Dean Prichard for proof-reading this manuscript. This work first appeared in the author's Ph.D. thesis.[2]

REFERENCES

1. L.-S. Luo, H. Chen, S. Chen, G. D. Doolen, and Y. C. Lee, *Phys. Rev. A* **43**:7097 (1991).
2. L.-S. Luo, Ph.D. thesis, Georgia Institute of Technology, 1993.
3. S. P. Das, H. J. Bussemaker and M. H. Ernst, *Phys Rev. E* **48**:245 (1993).

4. P. Grosfils, J. P. Boon, R. Brito and M. H. Ernst, *Phys. Rev. E* **48**:2655 (1993).
5. O. Behrend, R. Harris and P. B. Warren, *Phys. Rev. E* **50**:4586 (1994).
6. U. Frisch, B. Hasslacher, and Y. Pomeau, *Phys. Rev. Lett.* **56**:1505 (1986).
7. S. Wolfram, *J. Stat. Phys.* **45**:471 (1986).
8. U. Frisch, D. d'Humières, B. Hasslacher, P. Lallemand, Y. Pomeau, and J.-P. Rivet, *Complex Systems* **1**:649 (1987).
9. G. D. Doolen, editor, *Lattice Gas Methods for Partial Differential Equations* (Addison–Wesley, Redwood City, CA, 1990).
10. G. R. McNamara and G. Zanetti, *Phys. Rev. Lett.* **61**:2332 (1988).
11. P. J. Davis, *Circulant Matrices* (Wiley, New York, 1979).
12. L. P. Kadanoff, G. R. McNamara, and G. Zanetti, *Complex Systems* **1**:791 (1987).
13. W. H. Press, S. A. Teukolsky, W. T. Vetterling, and B. P. Flannery, *Numerical Recipes in Fortran* (Cambridge, New York, 1992), 2nd Edition, Chapter 12.
14. K. Huang, *Statistical Mechanics* (Wiley, New York, 1963).
15. M. Ernst and T. Naitoh, *J. Phys. A* **24**:2555 (1991).
16. J. C. Maxwell, *Philos. Trans. Roy. Soc. London* **170**:231 (1879).
17. D. K. Bhattacharya and G. C. Lie, *Phys. Rev. Lett.* **62**:897 (1989).
18. G. Mo and F. Rosenberger, *Phys. Rev. A* **42**:4688 (1990).
19. I. Ginzbourg and P. M. Adler, *J. Phys. II France* **4**:191 (1994).
20. B. J. Alder and W. E. Alley, *Phys. Rev. A* **1**:18 (1970).
21. B. J. Alder and W. E. Alley, *Phys. Today* **37**(1):56 (1984).